Journal of Materials Chemistry C

Electrodeposition of Nanometer-Thick Epitaxial Films of Silver onto Single-Crystal Silicon Wafers

Journal:	*Journal of Materials Chemistry C*
Manuscript ID	TC-ART-11-2018-006002.R2
Article Type:	Paper
Date Submitted by the Author:	10-Jan-2019
Complete List of Authors:	Chen, Qingzhi; Missouri University of Science and Technology, Chemistry Switzer, Jay; Missouri University of Science and Technology, Chemistry and Graduate Center for Materials Research

Electrodeposition of Nanometer-Thick Epitaxial Films of Silver onto Single-Crystal Silicon Wafers

Authors: Qingzhi Chen and Jay A. Switzer*

Affiliations:

Missouri University of Science & Technology, Department of Chemistry and Graduate Center for Materials Research, Rolla, MO 65409-1170, USA.

*Correspondence to: jswitzer@mst.edu

Abstract:

Silver films were deposited epitaxially for the first time onto low-index, single-crystal silicon wafers through an electrochemical method in an aqueous silver acetate bath. A negative potential of -2.34 V vs. Hg/Hg_2SO_4 was used for both pre-polarization and during the deposition to avoid Si oxidation. The epitaxy of Ag films on Si(111), (110) and (100) was characterized by X-ray diffraction symmetric scans and pole figures. The Ag films showed [111], [110] and [100] out-of-plane orientations, respectively, with in-plane order determined by the Si substrates. Interface models consistent with the observed orientations invoke coincident site lattices (CSLs), in which four unit meshes of Ag coincide with three unit meshes of Si. These CSLs reduce the lattice mismatch from -24.9% to +0.13%. A thickness of about 10 nm was obtained for Ag deposited for ten minutes. A comparison of silver acetate electrolyte and cyanide electrolyte was also performed, showing advantages of the acetate bath over the cyanide bath for growth of epitaxial films of Ag on Si surfaces.

1 Introduction

Silver (Ag), a coinage metal possessing the highest electrical conductivity, has been one of the most important metals for the electronic industry for decades. Beyond that, its ability to from a Schottky barrier with n-type silicon qualifies it as a potential candidate for electrical or photovoltaic devices, and its excellent optical properties make it ideal for plasmonic devices and surface enhanced Raman spectroscopy (SERS) substrates [1–5]. However, the use of Ag deposited on other substrates taking advantages of its optical properties requires a major characteristic: epitaxy (or single crystallinity), since the grain boundaries in a polycrystalline Ag film cause extra scattering and absorption losses [2,5]. The frequently used techniques for Ag deposition such as vacuum evaporation and chemical vapor deposition (CVD) often give polycrystalline Ag [6,7]. Although there have been examples of epitaxial growth of Ag on Si through magnetron sputtering and molecular beam epitaxy (MBE) [8–13], these techniques require high vacuum and the MBE equipment is expensive, with limited access to most researchers. Inspired by Allongue's work in epitaxial electrodeposition of Au on Si [14], we herein introduce a method that directly electrodeposits Ag epitaxially on three different orientations of Si substrates using a simple aqueous electrolyte solution. We have previously shown that Au deposited on Si with different orientations can be used as a low-cost proxy for single-crystal Au, and as a photoanode for photoelectrochemical regenerative cells [15,16], we have also shown that Cu deposited on Si(100) could serve as a proxy for single-crystal Cu(100) as well[17]. Ag epitaxially

deposited on Si could have a broader impact due to its lower cost than Au, and because Ag exhibits a wider range of applications from plasmonic devices, to surface catalysts, to highly selective absorbers/emitters [18]. We also compare the morphology and epitaxy of films deposited from standard cyanide baths[18] with those deposited from the simple acetate bath.

2 Experimental

Si wafer etching process and Ag deposition. N-type Si wafers with [111], [110] and [100] orientations were used as substrates for Ag deposition. The resistivity of the Si wafers was approximately 1 Ω·cm. The wafers were purchased from Virginia Semiconductor Inc. and were hydrogen-terminated before use. Wafers were etched in 5% HF acid for 3 minutes to remove the native oxide layer, and then soaked in 90 °C DI water for 15 min to form an SiO_x layer, then etched again with 5% HF acid for 30 s. Gallium-indium eutectic was applied to the back of the Si wafers to form an ohmic contact, followed by silver wire and silver print II (GC electronics) as a back contact. Silicone sealant or melted Apiezon Type W wax was used to insulate the back and edges of the Si substrates. The Ag films were directly electrodeposited onto the Si substrate using a "hot-wire" method. That is, a prepolarized potential was applied to the electrode before the immersion of the sample into the solution to prevent the oxidation of Si in the aqueous environment. The plating solution contained 0.1 mM AgOAc, 1 mM KOAc, 1 mM H_2SO_4 and 0.1 M K_2SO_4, where 90

ml DI water was added to 10 ml stock solution containing 1 mM AgOAc, 10 mM KOAc and 10 mM H_2SO_4. The pH of the solution was 3.6. The polarization curves of a Au electrode in the electroplating solution were obtained by performing linear sweep voltammetry (LSV) scans from the open circuit potential (OCP) towards negative potentials at a scan rate of 10 $mV \cdot s^{-1}$. A potential of -2.34 V vs. Hg/Hg_2SO_4 electrode was used for Ag prepolarization and deposition at room temperature. The cyanide plating solution was made by dissolving 2.4 mM AgCl in a solution containing 8.5 mM KCN, followed by adding 0.1 M K_2CO_3 as a supporting electrolyte. The pH of the solution was 11. A prepolarized potential of -1.9 V vs. Ag/AgCl electrode was used for Ag deposition in the cyanide bath at room temperature. Note that the AgCl reference electrode was not used in the acetate bath to avoid precipitation of AgCl. Both EG&G Model 273A and Autolab 30 potentiostats were used for Ag deposition and measurements.

X-ray diffraction measurements and SEM Measurements. The XRD measurements were done using a Philips X'Pert Materials Research diffractometer with a Cu Kα_1 radiation source. A crossed slit collimator with 2 mm divergence slit and 2 mm mask with a Ni filter and a 0.27° parallel plate collimator were used for X-ray pole figure measurements. The SEM images were obtained using a FEI Helios Nanolab Dualbeam microscope with accelerating voltages ranged from 5 to 15 kV.

3 Results and Discussion

The LSV curve of a Au-coated glass electrode in the stirred AgOAc plating solution towards negative potentials shows mainly four regions, as shown in Figure 1. Region I is the Ag(I) reduction step, where Ag metal starts depositing at about -0.1 V vs. Hg/Hg_2SO_4, and reaches the limiting current of about 0.04 mA cm^{-2} due to the forced convection. The second region is attributed to oxygen reduction reaction (ORR), and the regions III and IV correspond to proton reduction and water reduction reactions, respectively. The deposition of Ag on Si wafers was conducted by applying a static potential of -2.34 V, where a Faradic efficiency is estimated to be 0.22% by comparing the limiting current density at region I to the current observed at the deposition potential (-2.34 V). The large negative potential was used to avoid Si oxidation and to evolve hydrogen, which has been reported to contribute to a more uniform nucleation and more smooth growth for electrodeposited metals [14,20-21]. The applied potential corresponds to a 2.26 V overpotential for the reduction of Ag(I) to Ag, a 1.49 V overpotential for H_2 evolution, and a 0.62 V overpotential for the reduction of SiO_2 to Si.

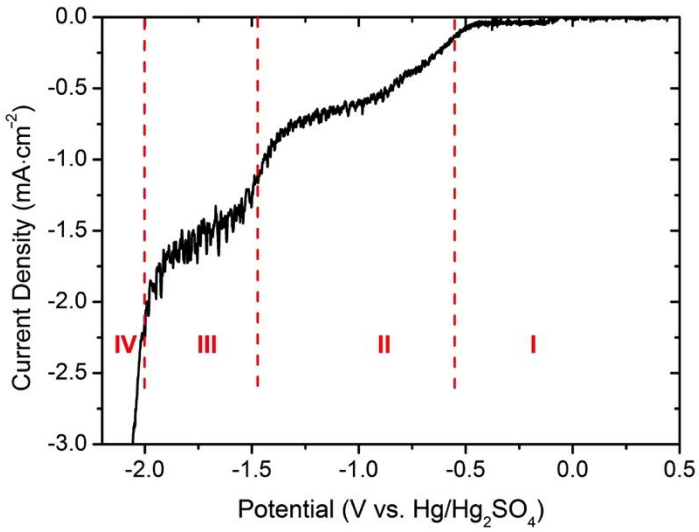

Fig 1. Linear sweep voltammogram of a Au electrode in the stirred acetate-based Ag plating solution at a scan rate of 10 mV s^{-1}.

The SEM images of Ag deposited on Si(111) at different deposition times offer a snapshot of the Ag growth progress. As shown in Figure 2 (a), Ag deposited for 1 min exhibits 3D island growth. The 3D island growth is followed by 2D growth producing a fractal pattern (Figure 2B). After 10 minutes of deposition the Ag film has coalesced into a dense film (Figure 2C) covered with larger Ag islands with sizes ranging from 20 nm to several hundred nm. As can be seen in Figure 2, the films deposited for short times have a larger density of islands than films deposited for longer times. This could be due to loss of islands due to poor Ag/Si adhesion, or to the merging of small islands to produce larger islands. More work is needed to determine the reason for the lower density of islands on the films deposited for longer times.

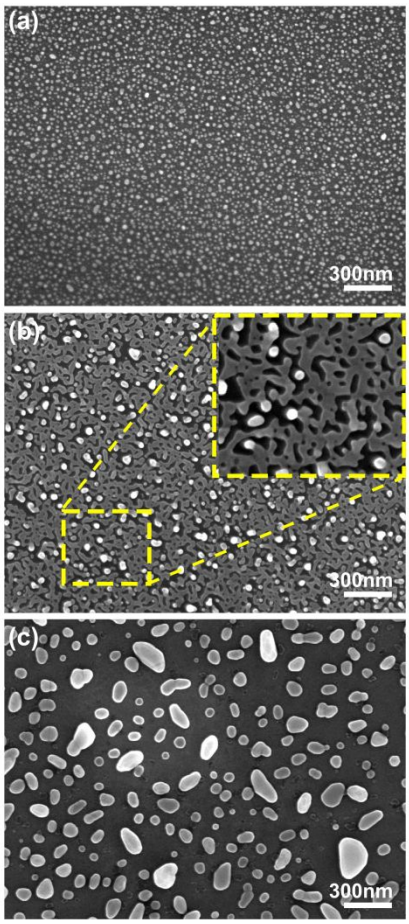

Fig 2. SEM plan-view images of silver thin films deposited from the acetate bath on Si(111) for different deposition times. (a) 1 min deposition, (b) 5 min deposition and (c) 10 min deposition. The higher magnification inset in (b) shows the fractal structure of the Ag.

To determine the epitaxial relationships between the electrodeposited Ag and the Si substrate, XRD symmetric 2-theta scans and pole figure scans were obtained. Figure 3 (a) shows the 2-theta scan of Ag deposited for 10 min on Si (111). As shown in the plot, only Ag (111) and (222) peaks were observed. This indicates a strong out-of-plane orientation. A detailed slow-rate scan of the Ag (111) peak shows two satellite peaks (interference fringes) from Laue oscillations. A thickness of 10.1 nm was calculated from the position of the satellite peaks (see the supplementary information for details). The (222) d-spacing was 0.11783 nm, compared with

0.11774 nm for bulk Ag. Hence the Ag d-spacing is larger than expected out-of-plane, indicative of uniform in-plane compressive strain. The in-plane orientation of Ag on Si is revealed by X-ray pole figures. In Figure 3 (c), the Si (220) pole figure shows three spots separated azimuthally by 120°at a tilt angle of 35.5°, consistent with the (220) crystalline plane projection in a single crystalline Si(111). However, in Figure 3(d), the Ag (220) pole figure shows six spots separated azimuthally by 60° at a tilt angle of 35.5°. The additional three spots can be interpreted as coming from 180° rotational twins of Ag. This twinning phenomenon occurs also during the deposition of other fcc metals such as Au on Si [15]. The full width at half maximum (fwhm) in the azimuthal angle in the pole figure was 4.85°. The epitaxial relationships consistent with these pole figures are Ag(111)[10-1]||Si(111)[10-1] and Ag(111)[-101]||Si(111)[10-1].

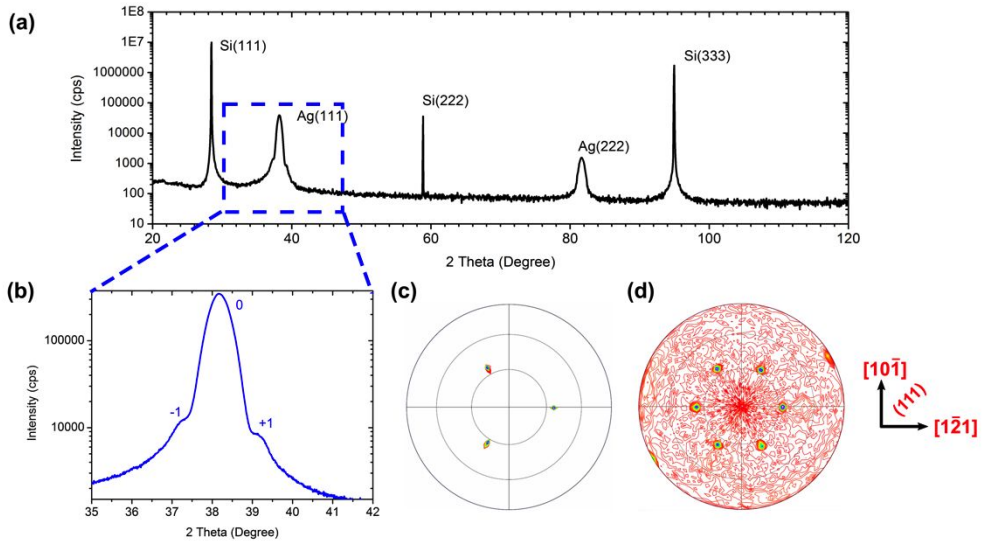

Fig 3. X-ray diffraction of Ag deposited on Si(111) from the acetate bath. (a) 2 theta gonio scan, showing {111} out-of-plane growth of the silver film, (b) detailed scan of silver (111) peak, showing ±1 orders of Laue oscillation peaks, (c) the Si (220) pole figure, and (d) Ag (220) pole figure showing in-plane orientations.

Silver deposition on Si wafers with other orientations using the same electrolyte also produced epitaxial films. Figure 4 (a) shows the 2 theta scan of Ag deposited for 5 min on the Si(110) surface. Similar to the Ag film on Si(111), the silver deposited on Si (110) also shows a (220) peak only, which follows the out-of-plane orientation of the silicon substrate. The (220) d-spacing was 0.14445 nm, compared with 0.14420 nm for bulk Ag, consistent again with uniform in-plane compression. The Si (111) pole figure in Figure 4 (b) shows two spots separated azimuthally by 180° at a tilt angle of 35.0° as expected, while the silver (111) pole figure in Figure 5 (b) also shows two major spots at the same tilt angle. However, there are four additional spots at a tilt angle of 57.0° and two more spots at 75.0°. These extra spots come from the (411) twins that were deposited simultaneously during the (110) growth of the Ag film. A detailed discussion about the twinning phenomenon on Si(110) can be found in the supplementary materials. The fwhm in the azimuthal angle in the pole figures was 7.34^{o}. The deposition was also performed for 5 min on the Si(100) surface. The 2 theta scan in Figure 5 (a) of the Ag deposited on Si(100) only shows a minor (200) peak, indicating a slower growth rate under the experimental condition compared to that of the Si(110) surface. The (200) d-spacing was 0.20414 nm, compared with 0.20390 nm for bulk Ag, consistent again with uniform in-plane compressive strain. Although little material was obtained, the pole figures still show an in-plane ordered growth of silver on Si(100). Figure 5 (b) shows the Si (111) pole figure, presenting four spots separated evenly at a tilt angle of 54.7° consistent with the tilt angle between the [111] and [100] directions in the cubic crystal system. In Figure 5 (c), a

Ag (111) pole figure also shows four spots at the same position as those in the Si (111) pole figure. The fwhm in the aximuthal angle in the pole figure is 7.67°. The epitaxial relationships with Ag on Si (110) and (100) are Ag(110)[1-10]||Si(110)[1-10] and Ag(100)[011]|| Si(100)[011].

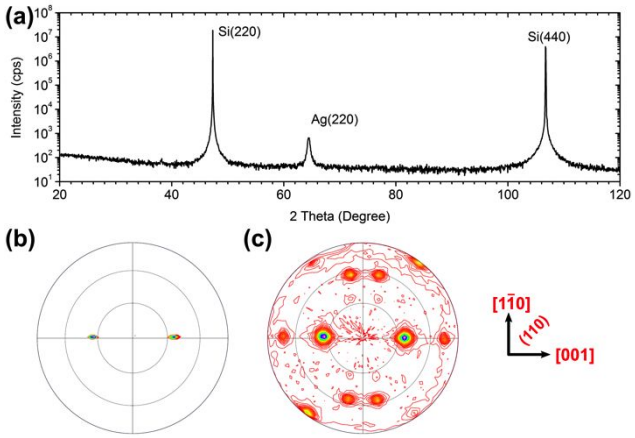

Fig 4. X-ray diffraction of Ag deposited on Si(110) from the acetate bath. (a) 2 theta gonio scan, showing only {110} out-of-plane growth of the Ag film, (b) Si (111) pole figure and, (c) the Ag (111) pole figure with in-plane orientations.

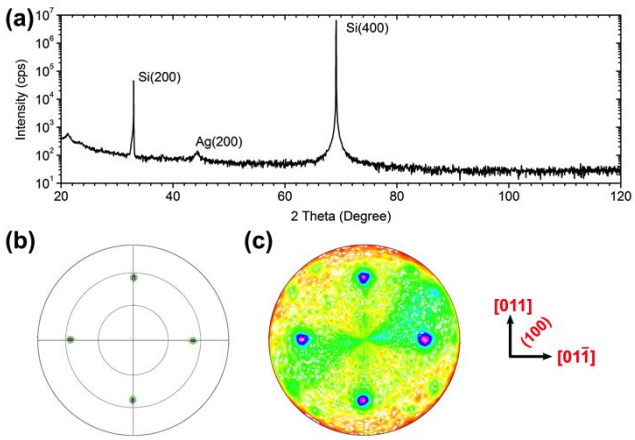

Fig 5. X-ray diffraction of Ag deposited on Si(100) from the acetate bath. (a) 2 theta gonio scan, showing a low-intensity (200) peak of the Ag film, (b) the Si (111) pole figure and, (c) the Ag (111) pole figure with the in-plane orientations.

Interface models can shed light on the Ag epitaxial growth on Si. The original $1d_{Ag}$ x $1d_{Si}$ lattice generates a mismatch of -24.9%, which is typically too high for epitaxial growth. However, the formation of coincident site lattices (CSL) reduces the Ag-Si mismatch to 0.13%. As shown in the interfacial models in Figure 6, the CSL is made up by 4 unit meshes of Ag lattice coinciding with 3 unit meshes of Si lattice, and is represented by the red triangles/rectangles. These CSLs help reduce the strains so that the Ag film deposited on Si will not shrink, flake off or be forced to conduct an in-plane rotation to avoid the huge mismatch like Cu on Si [17,22-23]. Note that the same CSL was invoked to explain the epitaxial electrodeposition of Au on Si(111) by Munford *et al.*[24] and the electron beam evaporation of epitaxial Ag nanoclusters on Si by Li and Zuo [25] . Das and co-workers also developed this CSL using first principle simulations to reduce the effective strain [26]. Note that our X-ray results also showed that the films had slightly larger out-of-plane d-spacings than bulk Ag, consistent with the in-plane compressive stress predicted by the CSL.

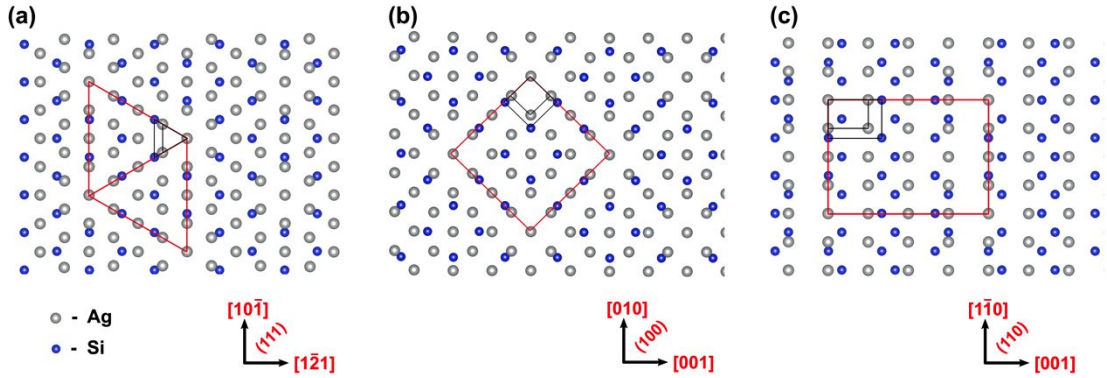

Fig 6. Interfacial models of Ag on Si showing the formation of the Ag-Si coincident site lattices (CSL) in which 4 unit meshes of Ag coincide with 3 unit meshes of Si. (a) Ag on Si(111), (b) Ag on Si(100) and (c) Ag on Si(110). The red triangles/rectangles

represent to the CSLs and the black ones represent to the large-mismatch 1 x 1 lattices.

To compare the method above to the conventional cyanide bath plating method and as an attempt of acquiring smoother Ag deposits, a cyanide plating electrolyte was also made and Ag films were deposited on the three different orientations of Si. A LSV study of a Au electrode in the cyanide bath was also conducted and is shown in Figure S1 in the supplementary materials. The LSV curve shows that the Ag starts to deposit at a potential of -0.4 V vs. Ag/AgCl. The deposition potential was chosen to be -1.9V, which 1.53 V negative of the silver-cyanide complex reduction potential, to avoid potential Si oxidation as well. The SEM was also used to characterize the surface morphology of the deposited silver films. In Figure 7 (a), the 10 s deposited Ag grows mainly as particles and has not achieved coalescence on the Si surface. It grows into a dense film after one minute, as shown in Figure 7(b). The increased growth rate compared to the silver films deposited from acetate bath could be attributed to the higher concentration (2.4 mM vs. 0.1 mM for the acetate bath). Also the grain size of the thicker silver film from the cyanide bath is more uniform compared to that from the acetate bath, which indicates that it is more likely to obtain compact and uniform films in the cyanide bath for thicker deposits. The X-ray diffraction shows that the Ag film deposited on Si(111) in the cyanide bath is epitaxial with the Si as well. As shown in Figure 7(c), the 2 theta scan gives only the {111} family of peaks for the silver deposit. Furthermore in Figure 7(d) and (e), the pole figures show the same patterns as those deposited in the acetate bath, giving an

epitaxial relationships of Ag(111)[10-1]||Si(111)[10-1] and Ag(111)[-101]|| Si(111)[10-1]. The fwhm in the aximuthal angle in the pole figures was 7.70°. However, the epitaxial growth of Ag on Si(110) and (100) surface using the cyanide bath was not successful. The 2 theta scans of silver deposits on these two silicon surfaces showed diffraction peaks from multiple crystalline orientations (see details in Figure S2 and S3 in the supplementary materials). This could limit the use of the cyanide bath for the epitaxial growth of Ag on Si (110) and (100).

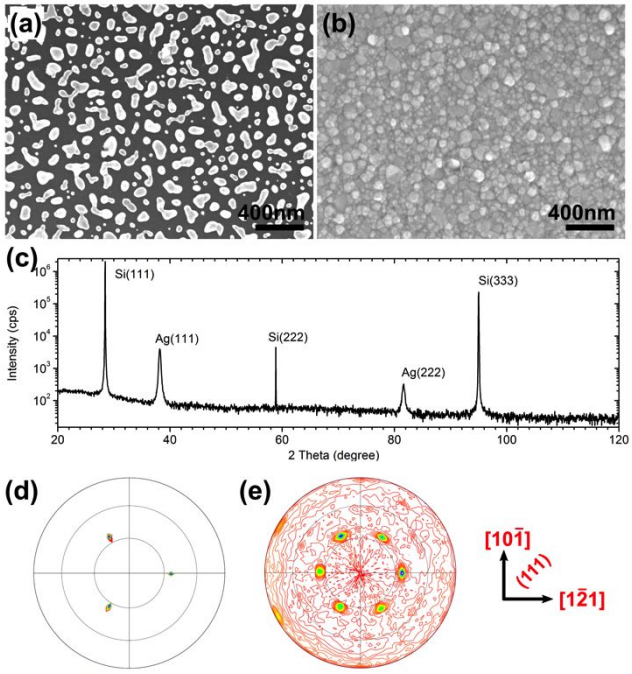

Fig 7. SEM images and the X-ray diffraction of Ag deposited Si(111) from the cyanide bath. (a) SEM image for 10 seconds silver deposition, (b) SEM image for 1 minute silver deposition, (c) the 2 theta gonio scan, showing only {111} out-of-plane growth of the silver film, (d) the Si (220) pole figure and (e) the Ag (220) pole figure with the in-plane orientations.

Hence, the cyanide plating bath works well for the electrodeposition of epitaxial films of Ag on Si(111), but it produces polycrystalline films on Si(100) and Si(110). One possible explanation for the polycrystalline growth on Si(100) and Si(110) is the

propensity of Ag to grow with a [111] orientation from the cyanide bath. The Ag will grow with a [111] fiber texture even on amorphous or polycrystalline substrates. This kinetically-controlled growth in the [111] direction is apparently stronger than the thermodynamically-controlled template effect of the substrates to grow epitaxial films. Figure S4 shows XRD 2 theta scans for thicker Ag films grown for 3 minutes on Si(100) and Si(110). In both cases, the Ag(111) peak is more intense than with the Ag(200) or Ag(220) peaks, suggesting kinetically-controlled fiber growth.

4 Conclusions

We show in this work that nm-thick Ag films can be electrochemically deposited epitaxially onto single-crystal Si. A key feature of the electrodeposition that allows for epitaxial growth is the use of a very negative pre-polarization and growth potential to prevent the oxidation of Si to amorphous SiO_x. Films deposited from the acetate bath follow the out-of-plane and in-plane orientation of Si(111), Si(110), and Si(100) wafers, whereas films deposited from the cyanide bath grow epitaxially on Si(111), but deposit as polycrystalline films on Si(100) and Si(110). This is attributed to the propensity of the Ag to grow with a [111] fiber texture from the cyanide bath. The large mismatch of -24.9% of the Ag/Si system is reduced to +0.13% by the formation of coincident site lattices (CSLs). In these CSLs, four unit meshes of Ag coincide with three unit meshes of Si. The compressive residual strain observed in the X-ray diffraction patterns is consistent with the CSL. The Ag films could serve as proxies

for Ag single crystals for the epitaxial growth of other materials. They could also be used as catalysts to study the different activities of various crystal planes of Ag. Low coverage deposits have a fractal geometry, which may yield large plasmonic responses.

Acknowledgements:

This material is based upon work supported by the U.S. Department of Energy, Office of Basic Energy Sciences, Division of Materials Sciences and Engineering, under Grant No. DE-FG02-08ER46518

References:

1 R. Balsano, A. Matsubayashi and V. P. Labella, *AIP Adv.*, 2013, **3**, 112110.
2 L. Sun, C. Zhang, C. Y. Wang, P. H. Su, M. Zhang, S. Gwo, C. K. Shih, X. Li and Y. Wu, *Sci. Rep.*, 2017, **7**, 3–8.
3 Y. J. Lu, J. Kim, H. Y. Chen, C. Wu, N. Dabidian, C. E. Sanders, C. Y. Wang, M. Y. Lu, B. H. Li, X. Qiu, W. H. Chang, L. J. Chen, G. Shvets, C. K. Shih and S. Gwo, *Science*, 2012, **337**, 450–453.
4 R. Lu, Y. Wang, W. Wang, L. Gu and J. Sha, *Acta Mater.*, 2014, **79**, 241–247.
5 Y. Wu, C. Zhang, N. M. Estakhri, Y. Zhao, J. Kim, M. Zhang, X. X. Liu, G. K. Pribil, A. Alù, C. K. Shih and X. Li, *Adv. Mater.*, 2014, **26**, 6106–6110.
6 W. Lin, T. H. Warren, R. G. Nuzzo and G. S. Girolami, *J. Am. Chem. Soc.*, 1993, **115**, 11644–11645.
7 A. Grodzicki, I. Łakomska, P. Piszczek, I. Szymańska and E. Szłyk, *Coord. Chem. Rev.*, 2005, **249**, 2232–2258.
8 K.-H. Park, G. A. Smith, K. Rajan and G.-C. Wang, *Metall. Mater. Trans. A*, 1990, **21A**, 2323–2332.
9 D. C. Mckenna, G. Wang and K. Rajan, *J. Electron. Mater.*, 1991, **20**, 1–6.
10 T. B. Hur, H. K. Kim, D. Perello, M. Yun, A. Kulovits and J. Wiezorek, *J. Appl. Phys.*, 2008, **103**, 1–6.
11 T. B. Hur, H. K. Kim and J. Blachere, *Phys. Rev. B - Condens. Matter Mater. Phys.*, 2007, **75**, 1–5.

12 D. Kong, L. Jiang and J. Drucker, *J. Appl. Phys.*, 2015, **118**, 213103.
13 A. Bhukta, P. Guha, A. Ghosh, P. Maiti and P. V. Satyam, *Appl. Phys. A Mater. Sci. Process.*, 2016, **122**, 1–8.
14 P. Prod'Homme, F. Maroun, R. Cortès and P. Allongue, *Appl. Phys. Lett.*, 2008, **93**, 171901.
15 J. A. Switzer, J. C. Hill, N. K. Mahenderkar and Y. C. Liu, *ACS Appl. Mater. Interfaces*, 2016, **8**, 15828–15837.
16 Q. Chen and J. A. Switzer, *ACS Appl. Mater. Interfaces*, 2018, **10**, 21365–21371.
17 C. M. Hull and J. A. Switzer, *ACS Appl. Mater. Interfaces*, 2018, **10**, 38596–38602.
18 Y. Duan, S. Rani, Y. Zhang, C. Ni, J. T. Newberg and A. V. Teplyakov, *J. Phys. Chem. C*, 2017, **121**, 7240–7247.
19 M. Schlesinger, in *Modern Electroplating*, Wiley-Blackwell, 5th edn., 2011, pp. 131–138.
20 K. Leistner, K. Duschek, J. Zehner, M. Yang, A. Petr, K. Nielsch and K. L. Kavanagh, *J. Electrochem. Soc.*, 2018, **165**, H3076–H3079.
21 P. Prodhomme, S. Warren, R. Cortès, H. F. Jurca, F. Maroun and P. Allongue, *ChemPhysChem*, 2010, **11**, 2992–3001.
22 L. Chen, L. Andrea, Y. P. Timalsina, G. C. Wang and T. M. Lu, *Cryst. Growth Des.*, 2013, **13**, 2075–2080.
23 C. A. Chang, J. C. Liu and J. Angilello, *Appl. Phys. Lett.*, 1990, **57**, 2239–2240.
24 M. L. Munford, F. Maroun, R. Cortès, P. Allongue and A. A. Pasa, *Surf. Sci.*, 2003, **537**, 95–112.
25 B. Q. Li and J. M. Zuo, *Surf. Sci.*, 2002, **520**, 7–17.
26 A. H. M. Abdul Wasey, R. Batabyal, J. C. Mahato, B. N. Dev, Y. Kawazoe and G. P. Das, *Phys. Status Solidi Basic Res.*, 2013, **250**, 1313–1319.

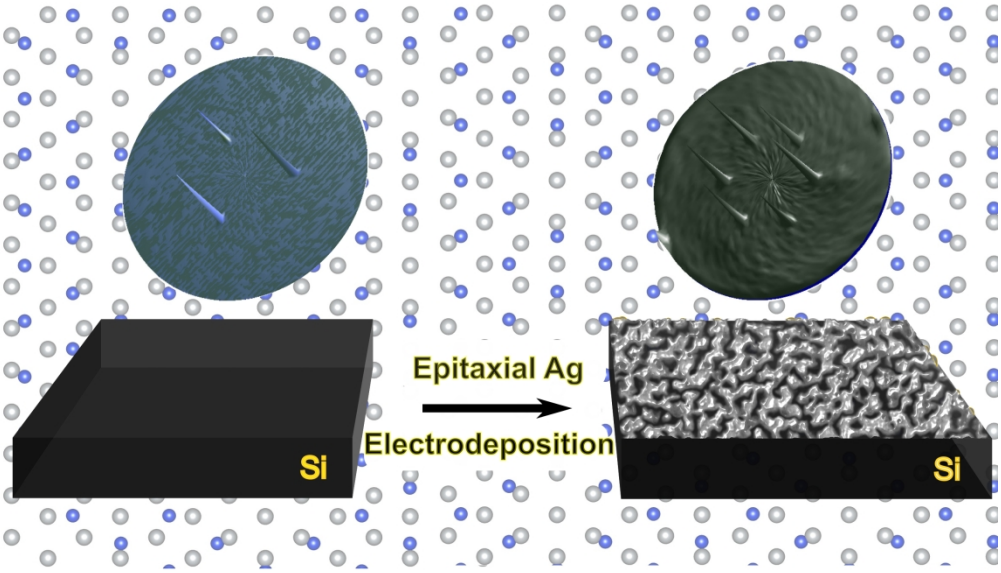
Epitaxial Ag
Electrodeposition
Si
Si